Supramolecular "Big-Bang" in single ionic surfactant/water system driven by electrostatic repulsions: From vesicles to micelles

Loïc Leclercq, Pierre Bauduin, Véronique Nardello-Rataj

Supramolecular “Big-Bang” in single ionic surfactant/water system driven by electrostatic repulsions: From vesicles to micelles

Loïc Leclercq,[a,] Pierre Bauduin,[b] and Véronique Nardello-Rataj,[a,]**

[a] Univ. Lille, UMR 8181 - UCCS - Unité de Catalyse et Chimie du Solide, F-59000 Lille, France.
[b] Institut de Chimie Séparative de Marcoule, UMR 5257, CEA/CNRS/UM2/ENSCM, BP 17171 CEA Marcoule, F-30207 Bagnols-sur-Cèze, France.

RECEIVED DATE

Abstract. In aqueous solution, dimethyl-di-*n*-octylammonium chloride, **[DiC$_8$][Cl]**, forms spontaneously dimers at low concentrations (1-10 mM) in order to decrease the hydrophobic/water contact. Dimers represent ideal building blocks for the abrupt edification of vesicles at 10 mM. These vesicles are fully characterized by dynamic and static light scattering, self-diffusion NMR and freeze-fracture transmission electron microscopy. An increase in concentration leads to electrostatic repulsions between vesicles which explode into small micelles at 30 mM. These transitions are detected by means of surface tension, conductivity and solubility of hydrophobic solutes as well as by isothermal titration microcalorimetry. These unusual supramolecular transitions emerge from the surfactant chemical structure that combines two contradictory features: (i) the double chain structure tending to form low planar aggregates with low water solubility, and (ii) the relatively short chains giving high hydrophilicity. The well balanced hydrophilic-hydrophobic character of **[DiC$_8$][Cl]** is then believed to be at the origin of the unusual supramolecular sequence offering new opportunities for drug delivery systems.

Keywords. Double-tailed ammonium/ Dynamic and Static light scattering/ Self-diffusion NMR/ Freeze-fracture TEM/ Micelles to vesicles transition

Introduction.

Molecular assemblies allow the formation of complex and fascinating structures with new and interesting properties.[1-3] The supramolecular self-assembling and their resulting properties can be externally controlled with numerous stimuli (e.g., temperature, concentration, salt, pH, etc.).[4,5] Surfactants are typical examples of molecules which give supramolecular self-assemblies. For instance, the aggregation of ionic surfactants can be easily tuned by varying the concentration, the charge of the aggregates (salt effect), the temperature as well as their spontaneous curvature (or the molecular packing parameter).[6,7] In respect to this, aggregates as diverse as micelles (e.g., spheres, disks, ribbons, and elongated micelles), vesicles, bilayers, and hollow regular icosahedra can be obtained.[8-10] Sometimes, transitions of one structure into another offer interesting opportunities for drug delivery systems and for membrane protein reconstitution.[11] However, transitions from vesicles to micelles by increasing concentration are usually observed for surfactant mixtures systems such as carboxylic/carboxylate, cationic/anionic, phospholipid/surfactant, and surfactant/cosurfactant mixtures.[12-16] For instance, catanionic surfactants (obtained from equimolar mixing of cationic and anionic surfactants) form spontaneously stable vesicles which present reversible transitions between vesicles and micelles upon temperature or composition changes.[17] These transitions were clearly attributed to the balance between electrostatic, van der Waals, hydrophobic and steric forces.[17-19] However, the transition of stable vesicles to micelles remains unknown with a single surfactant/water system.

On the other hand, di-*n*-alkyldimethylammonium surfactants, **[DiC$_n$][X]** (where X is the counterion), are widely used in the field of phase transfer catalysis, biocides, immunosuppressing drugs, wetting and antistatic agents, etc.[20,21] In respect with their packing parameter, double-tail ammonium surfactants are known to readily form vesicles or lamellae.[22] For instance, in 1977, Kunitake and Okahata reported the formation of **[DiC$_{12}$][Br]** vesicles after dispersion and sonication in water.[23] However, it is noteworthy that energy input (sonication or heating) is not required to obtain vesicles: their formation is totally spontaneous.[24] Interestingly, the existence of transition between small unilamellar to large multilamellar vesicles (SUVs → LMVs) was clearly identified

for **[DiC$_{12}$][Br]** aqueous solution.[25] As the vesicles are highly charged (≈ 50% near the critical vesicle concentration, CVC)[25], we can suggest a tentative mechanism to explain this transition. Indeed, as more **[DiC$_{12}$][Br]** is added, there is an increase in the concentration of SUVs, as well as an increase in the electrostatic repulsions between them. Above a given **[DiC$_{12}$][Br]** concentration, the electrostatic repulsions between SUVs becomes strong enough to allow the formation of LMVs (i.e., onion-like vesicles). However, it is noteworthy that the disruption of the stable SUVs cannot occur because the electrostatic repulsions cannot overcome the van der Waals chain-chain interactions in the bilayers. As the strength of van der Waals interactions decreases with the alkyl chain length, we can assume that transition from vesicles to smaller structures (e.g., vesicles → micelles) can be expected. At this point, it is worth mentioning that **[DiC$_8$]** cation constitutes a borderline case between hydrotropes, ≤ **[DiC$_6$]**, and surfactants, ≥ **[DiC$_{10}$]**, leading to a contradiction between two features (i) the double chain structure tending to form planar aggregates with low water solubility, and (ii) the relatively short chains giving high hydrophilicity.[26] This balanced hydrophilic-hydrophobic character of **[DiC$_8$][Cl]** leads to a particular aggregation behavior with the formation of dimer at low concentrations, a transition to large aggregates at intermediate concentrations and finally to the formation of micelles at high concentrations. Vesicles are observed between 10 and 30 mM whereas micelles are observed for higher concentrations (> 30 mM, see Figure 1).[27]

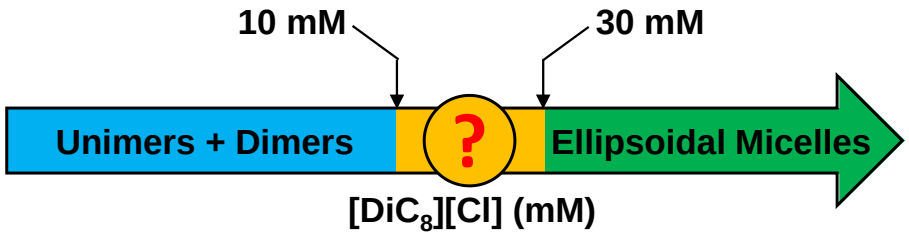

Figure 1. Structuration of dimethyl-di-*n*-octylammonium chloride, **[DiC$_8$][Cl]**, aqueous solution as a function of concentration.

In 2011, we reported Small-Angle Neutron Scattering (SANS) experiments which proved the formation of ellipsoid micelles above 30 mM.[28] However, the data obtained for aqueous solutions between 10 and 30 mM suggested discoid micelles (radius of 62.9 nm) or vesicles (radius of 102.5 nm). In consequence, we concluded that "*the precise structure of the large aggregate* [observed

between 10 and 30 mM] *cannot be resolved from the SANS results*".[28] To our knowledge, this result is rather uncommon as vesicle → micelle (or discoid micelle → ellipsoid micelle) transitions are usually exclusively observed with surfactant mixtures.[12-17] To go deeper into the structure of the large aggregates formed by **[DiC$_8$][Cl]** and to understand the origin of this unusual transition, we have combined in the present work solubilization of hydrophobic solutes, isothermal titration microcalorimetry, dynamic and static light scattering, self-diffusion NMR and freeze-fracture electron microscopy. Comparison of the data obtained by all these techniques has enabled to determine the exact nature of the aggregates formed in the 10-30 mM concentration range and the previous SANS results were further discussed in the light of the results achieved here. On the basis of the present results, a mechanism for this unusual transition could thus finally be proposed.

Results and discussion.

Preliminary investigations. To summarize our previous results obtained with **[DiC$_8$][Cl]**, the air/water surface tension (σ) and specific conductivity (κ, corrected for solvent) as a function of **[DiC$_8$][Cl]** concentration have been reported in Figures 2a and b.[27] These two techniques can give information on the transition between unimers (or dimers) and aggregates. The results were not in agreement with each other as two different critical concentrations were obtained at 12.0 ± 0.5 and 32.0 ± 0.5 mM. For the following discussion, the CAC obtained by surface tension and by conductivity measurements are represented, respectively, by CAC_1 (≈ 10 mM) and CAC_2 (≈ 30 mM). It is noteworthy that the specific conductivity also reveals that the aggregates formed between CAC_1 and CAC_2 is totally ionized whereas the aggregates above CAC_2 are partially ionized: the binding degree of the counterion are 0 and 0.46, respectively.

To get a better insight into the discrepancy between the CAC values, we performed solubility measurements of an hydrophobic dye (Sudan II) in the presence of increasing concentrations of **[DiC$_8$][Cl]** with or without NaCl (Figures 2c and 2d). As can be seen, the amount of dye solubilized at a **[DiC$_8$][Cl]** concentration below 10 mM is negligible and close to zero, proving the absence of aggregates. The first slight onset of solubilization is observed between 10.0 and 32.0 mM. These

values are in good agreement with the CAC_1 and CAC_2 values obtained from surface tension (12.0 mM) and from conductivity measurements (32.0 mM), respectively.

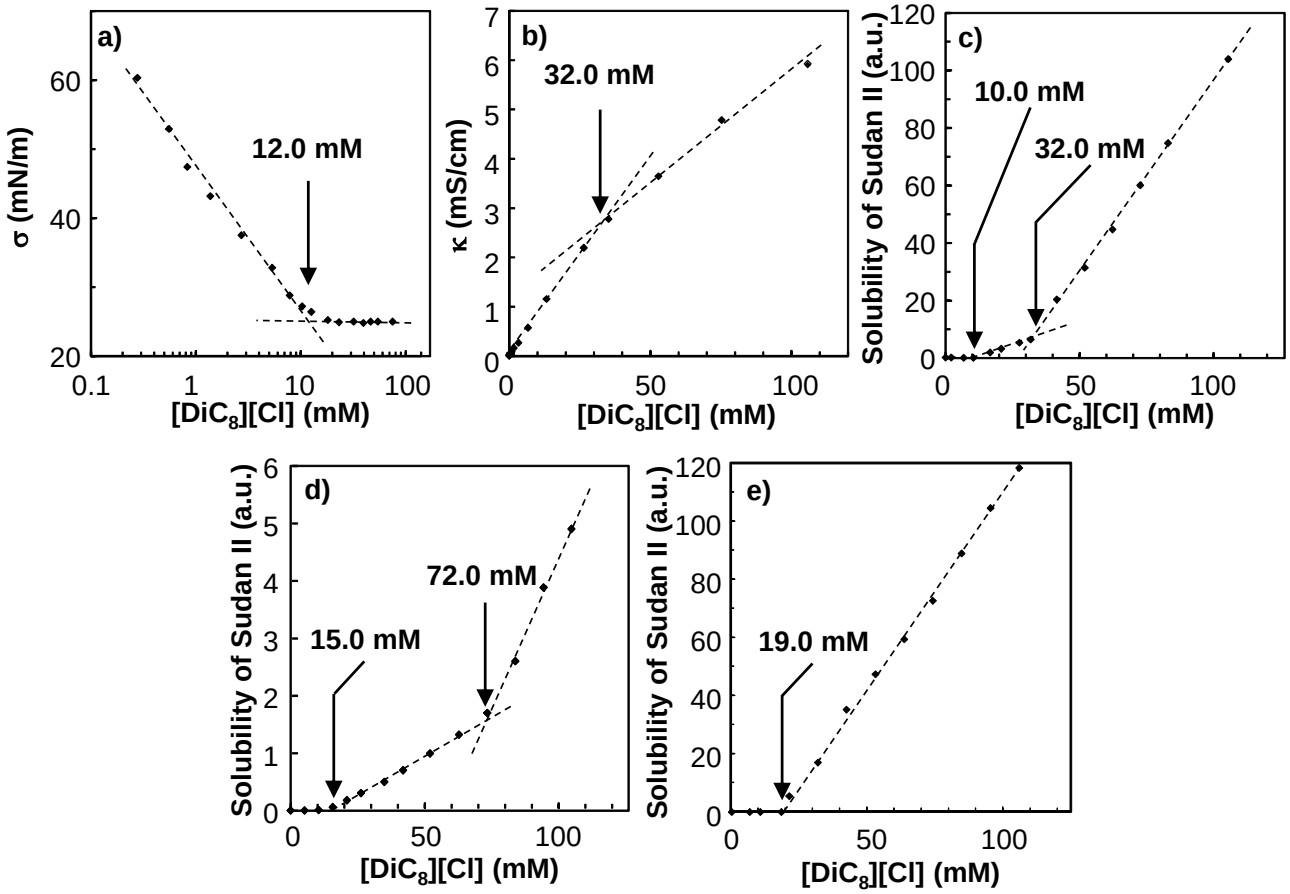

Figure 2. Surface tension, σ (a), specific conductivity, κ (b), solubility of Sudan II with NaCl = 0 M at 25.0 °C (c), solubility of Sudan II with NaCl = 0.1 M at 25.0 °C (d), and with NaCl = 0 M at 45.0 °C (e) as a function of **$[DiC_8][Cl]$** concentration (see experimental section for more details). Surface tension and conductivity data were taken from ref. 27.

Beyond CAC_2, a second regime is observed in which the dye solubilization is more efficient, i.e higher slope. This abrupt solubility increase above CAC_2 can be attributed the solubilization of hydrophobic dye molecules in the inner core of the micelle. In contrast, it is likely that the solubilization between CAC_1 and CAC_2 is related to the presence of larges aggregates. As the solubility enhancement is very weak, we can assume that the hydrophobic dye is solubilized in the aggregates formed in this concentration regime. The hydrophobic dye may be for example dissolved into the palisade layer of the large planar aggregates (i.e., discoidal micelles or vesicles) through

hydrophobic interactions. It is noteworthy that only ~1% of the **[DiC$_8$][Cl]** total concentration participates in the formation of the large aggregates between CAC$_1$ and CAC$_2$.[28] Therefore the dye solubility remains very weak in this region due to the low concentration of surfactant participating to the formation of the large aggregates. The presence of NaCl (0.1 M) has also a clear effect on the values of CAC$_1$ and CAC$_2$ (15 and 72 mM with NaCl *vs.* 10 and 32 mM without NaCl, compare Figures 2c and d). This seems to indicate that the large aggregates are stabilized by addition of salt. In contrast at 45 °C, only one transition is observed due to the disappearance of these large aggregates (see Figure 2e and the following discussion).

Next, isothermal titration microcalorimetry (ITC) experiments by dilution of a concentrated micellar solution show a complex evolution with a non-monotonic behavior (peaks) that is likely to be related to the complex mechanism of aggregation (Figure 3).

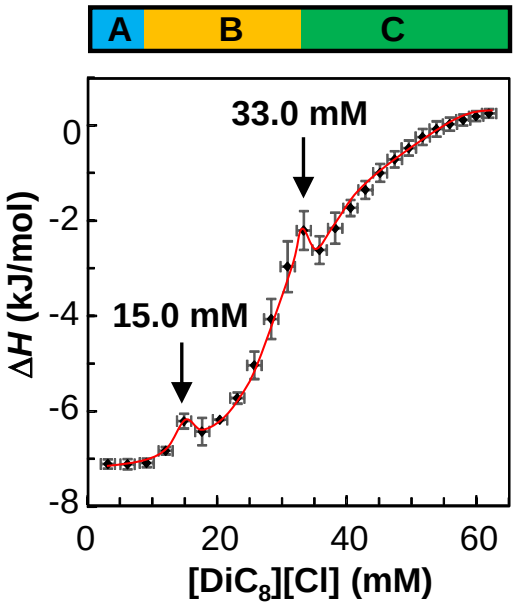

Figure 3. Variation of the enthalpy, ΔH, as a function of **[DiC$_8$][Cl]** concentration at 25.0 °C (see experimental section for more details).

As long as the solution concentration is high, only micelles are present. During the titration, the following reaction occurs successively depending on the **[DiC$_8$][Cl]** concentration (C, see Figure 3):

C < CAC$_1$: "micelles" → "unimers and dimers" (process **A**);

CAC$_1$ < C < CAC$_2$: "micelles" → "large aggregates" (process **B**);

C > CAC_2: “micelles” → “diluted micelles” (process **C**).

At a first order, the enthalpogram has a sigmoidal shape and the processes (**A**, **B** and **C**) are exothermic. In the beginning of the titration, we observe negative ΔH values for the dilution of concentrated **[DiC$_8$][Cl]** into water. For C < 10 mM, the dissociation of the micelles into unimers and dimers occurs (process **A**) and the observed ΔH values are almost constant below the CAC_1 (10 mM). Although the start of the aggregation process is rather easily determined from the ITC experiment, the end of aggregation is somewhat more difficult to determine precisely. However, we can consider that for concentrations higher than 60 mM, the dilution of the micelles is observed (process **C**). In a more detailed way, we observe the presence of two successive transitions around 15 and 33 mM. These specific concentrations are located close to the CAC_1 and CAC_2 values at which the **[DiC$_8$][Cl]** self-assembles into two different kinds of aggregates (see earlier discussion).

Dynamic light scattering (DLS). The **[DiC$_8$][Cl]** aggregates were investigated by dynamic light scattering (DLS). From a general point of view, aggregates in dispersion are in a constant random Brownian motion causing the intensity of scattered light to fluctuate as a function of time. For a large number of monodisperse aggregates, the correlation function ($g^2(\tau)$ - 1) can be expressed as an exponential decaying function of the correlator time delay (τ).

$$g^2(\tau) - 1 = \beta \exp(-2\Gamma\tau) \qquad (1)$$

where β is the intercept of the correlation function and Γ is the average characteristic line width. For spherical particles, Γ is related to the translational diffusion coefficient D provided that the internal motions are negligible. In the cumulant approach, the z-averaged translational diffusion coefficient was obtained from the average line width, Γ, based on the following equation:

$$\Gamma = Dq^2 \text{ with } q = \frac{4\pi n}{\lambda} \sin\left(\frac{\theta}{2}\right) \qquad (2)$$

where q is the magnitude of the scattering vector, n is the refractive index of dispersant, λ is the wavelength of the laser and θ is the scattering angle. DLS measurements were carried out at different scattering angles 30, 40, 50, 55, 60, 70, 80, 90, 95, 100, and 105° at 25 °C and at a fixed **[DiC$_8$][Cl]**

concentration of 20 mM. It is noteworthy that, each experiment was performed in triplicate and that, after preparation, the **[DiC$_8$][Cl]** aqueous solution was stored overnight at room temperature before performing DLS measurements. In each case, the auto-correlation functions can be fitted with a single exponential decay (eq. 1) for all investigated detection angles indicating a single diffusion mode observed with spherical aggregates (see the typical auto-correlation function presented in Figure 4a).

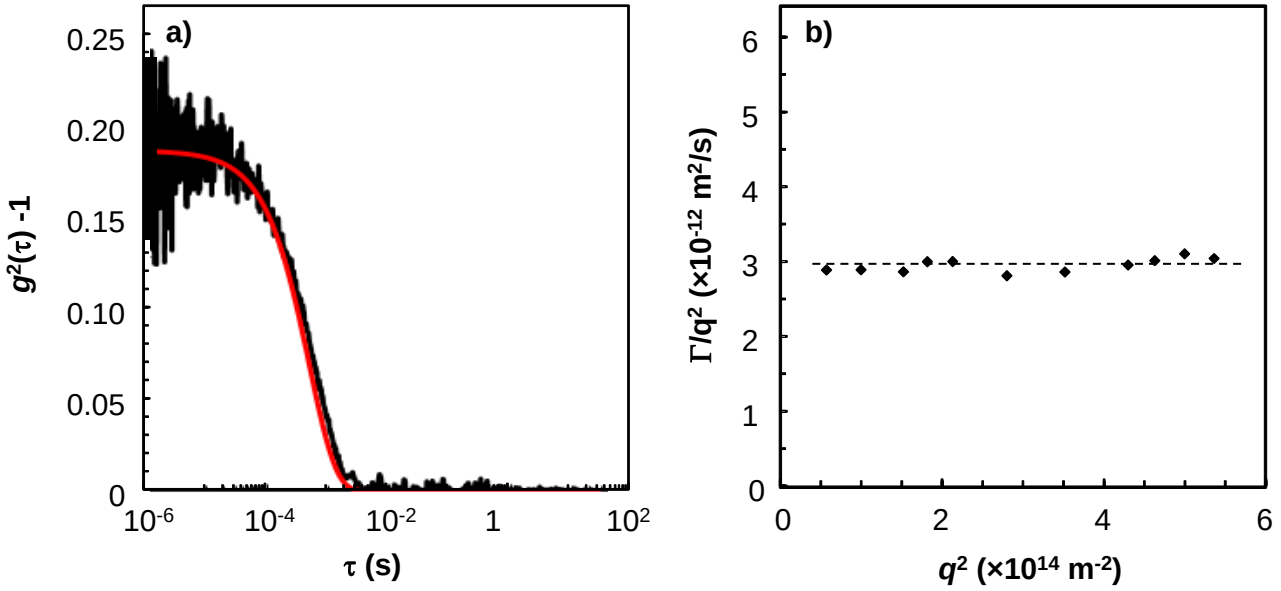

Figure 4. (a) Typical DLS auto-correlation functions for a 20 mM **[DiC$_8$][Cl]** aqueous solution at 25 °C with a detection angle of 80° (black) and curve fitting using eqs. 1 and 2 (red, fit parameter values: β = 0.1886 and Γ = 1009.46 s^{-1}). (b) Relationship between the scaled average characteristic line width (Γ/q^2) and the magnitude of the scattering vector (q^2) for a 20 mM **[DiC$_8$][Cl]** aqueous solution at 25 °C (detection angle: 30, 40, 50, 55, 60, 70, 80, 90, 95, 100, and 105°).

In order to confirm the spherical or the discoid structure of the aggregates formed between 10 and 30 mM, the relationship between the scaled average characteristic line width (Γ/q^2) and the magnitude of the scattering vector (q^2) have been plotted in Figure 4b. The Γ/q^2 values are constant and independent of the scattering angle, indicating a one mode diffusion typical of spherical shapes aggregates. The diffusion coefficient (D) is then estimated by $D = \Gamma/q^2$. The hydrodynamic radius (R_h) of the aggregates can be calculated from D by using the Stokes–Einstein equation.

$$R_h = \frac{kT}{6\pi\eta D} \quad (3)$$

where k is the Boltzmann's constant, T is the absolute temperature and η is the viscosity. R_h obtained by fitting the auto-correlograms is 85.9 ± 9 nm for all the investigated angles each in triplicate. It is noteworthy that the R_h values are very similar for **[DiC$_8$][Cl]** aqueous solution between 10 and 30 mM: 82.4, 89.2 , 106.7, and 63.4 nm (S.D.: ± 18%) for 10, 15, 25 and 30 mM, respectively. Moreover, the presence of NaCl (0.1 M) for a 20 mM **[DiC$_8$][Cl]** aqueous solution at 25 °C has a clear effect on the R_h values (134 ± 16 nm with NaCl *vs.* 85.9 ± 9 nm without NaCl).

Static light scattering (SLS). Static Light Scattering (SLS) was used to measure the scattering curve $I_s(q)$ which contains information about the scattering particle's size and its shape (see Figure 5a).

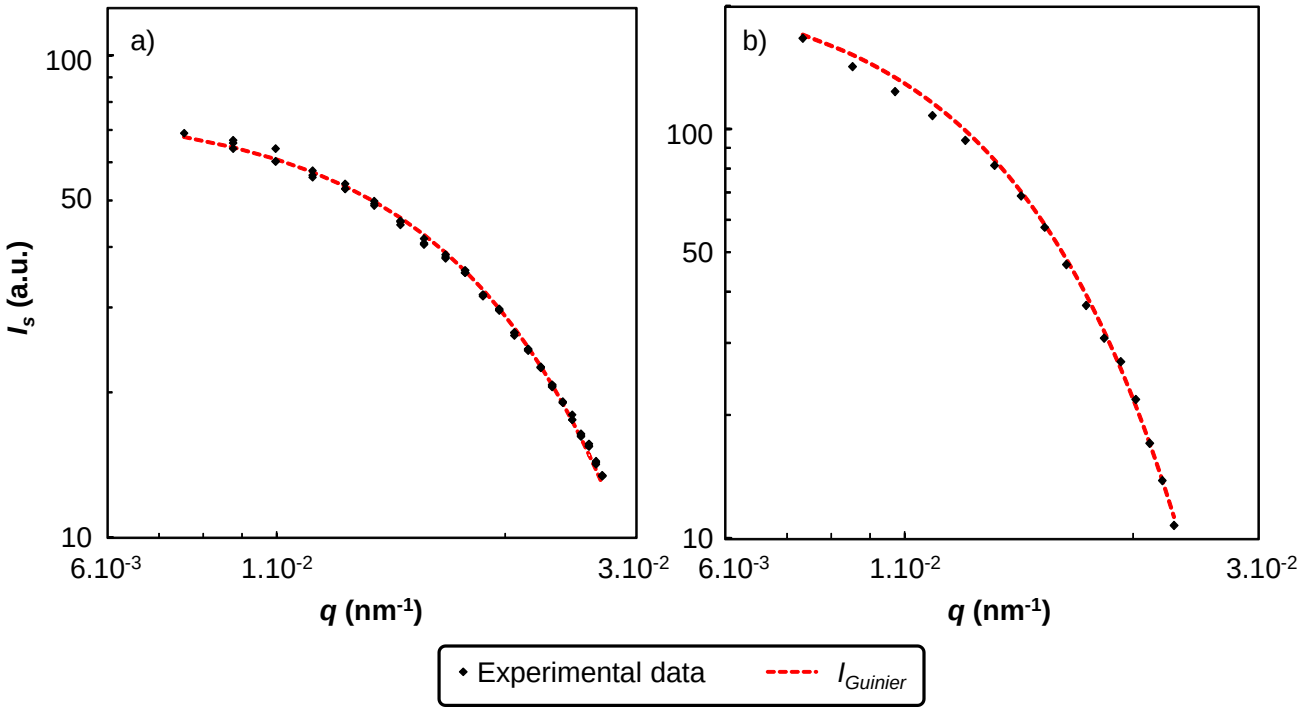

Figure 5. Experimental (◆) and fitted (dashed line, see eq. 4) SLS spectra for a 20 mM **[DiC$_8$][Cl]** aqueous solution at 25 °C without (a) or with NaCl (0.1 M, b).

The Guinier approximation was used to determine the radius of gyration (R_g) by fitting the scattering spectra:

$$I_s(q) = I_0 \exp\left(-\frac{R_g^2 q^2}{3}\right) \qquad (4)$$

Here, the best fit is obtained for R_g = 86 ± 5 nm (see the red dashed line in Figure 5). Further information on the aggregate structure can be obtained by the R_g/R_h, ratios. Indeed, hollow spheres (vesicles), cylinders, and rods give typical R_g/R_h values of 0.775, 1.0, 1.7, and >2.[29] For 20mM, the R_g/R_h ratio is indeed 1.0 which suggesting that the scattering objects are vesicles. All the presented results support the formation of spherical vesicles between 10 and 30 mM. Moreover, as the scattered intensity decreases very abruptly for concentrations above CAC_2 (see Figure 6a) it can be assumed that the vesicles (i.e., the main contributor to the scattered intensity compared to dimer and micelles) disappear in a very narrow range of concentrations Increasing the temperature also leads to disrupt the vesicles (20 mM of **[DiC$_8$][Cl]**) above around 20°C (see Figure 6b).

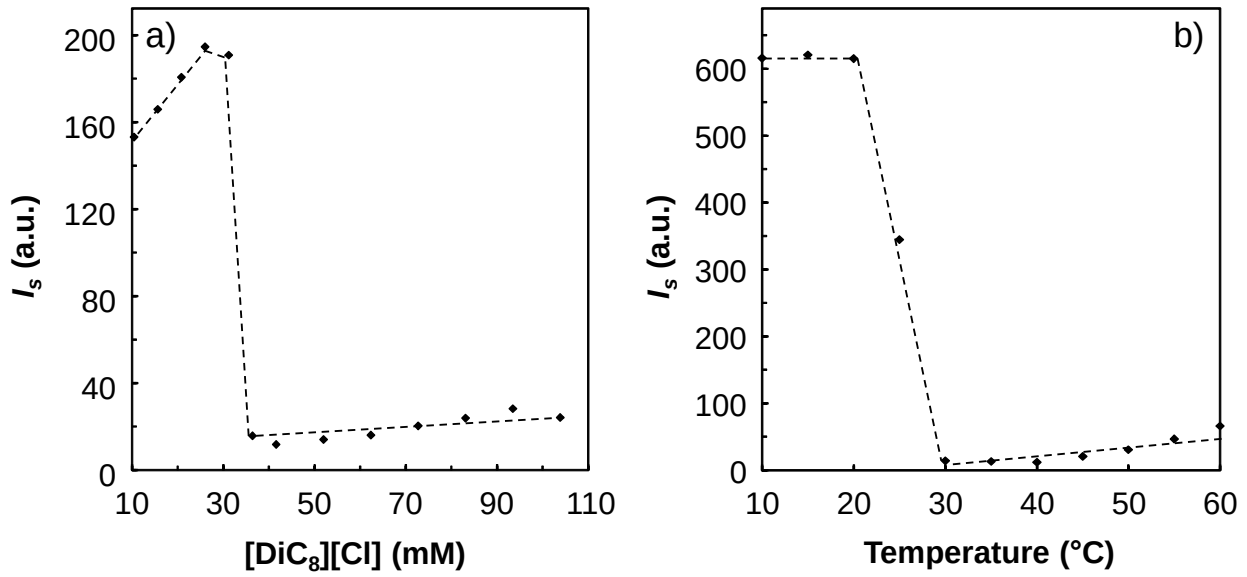

Figure 6. SLS scattered intensity, I_s, as a function of **[DiC$_8$][Cl]** concentration at 25 °C (a) and as a function of temperature for 20 mM of **[DiC$_8$][Cl]** (b) (detection angle: 90° with equal attenuation for each curves).

These results support the solubility of Sudan II at 25 and 45 °C which showed that the intermediate concentration zone, where vesicles are formed, vanished at high temperatures (see previous discussion). The presence of NaCl (0.1 M) produces a significant increase in the vesicle size. Indeed, the best fit of the SLS spectrum is obtained for R_g = 130 ± 16 nm (see the red dashed line in Figure

5b and eq. 4). As the R_h obtained by fitting the auto-correlograms is 134 ± 16 nm for all the investigated angles with 0.1 M of NaCl, the value of the R_g over R_h ratio is 0.97, which is again close to unity the value expected for hollow spheres (vesicles). As the R_g/R_h values are close with or without NaCl (1.0 and 0.97, respectively), the evolution of the 2nd virial coefficient by adding salt can be neglected compared to the effective change in the vesicle size. Therefore, the fit with a Guinier model in this region is sufficient. In our case, the increase in the size of the vesicles by adding salt is apparently totally related to a screening effect of the electrostatic repulsions acting between the charged polar head of the surfactant. This effect leads to decrease the average area per polar head in the vesicles which promotes a stronger charge compensation by the counterions. The decrease in the electrostatic repulsions leads to decrease the free energy difference between the vesicles and the micelles formed at higher concentrations as suggested by the extension of the realm of existence of the vesicles observed experimentally (see Figure 2e and the discussion below in the supramolecular speciation section).

Water self-diffusion coefficient. In order to support SLS and DLS results, water self-diffusion measurements were performed for three **[DiC$_8$][Cl]** concentrations 18, 20 and 22 mM. From a theoretical point of view, in the case of vesicles, self-diffusion coefficients of water can be linked to the behavior of two types of water molecules: inside (entrapped water) and outside of the vesicles (bulk water). Depending on the relation between the NMR time scale and vesicle permeability (the vesicles are not always completely impermeable), two water signals can be observed or be averaged to a unique signal. The NMR time scale is intrinsically related to the distance traveled by molecules. In the case of monodisperse vesicles, if the NMR time scale is small, the water molecules will have a diffusivity similar to that of bulk water because the water molecules do not collide the vesicle wall. In this case only one signal will be detected. In contrast, if the NMR time scale is large, the water molecules diffuse more slowly than bulk water because at this time scale water molecules can be collided a few times with the vesicle wall. Then, two cases can then occur: (i) if the vesicles are impermeable (i.e., multilamellar vesicles), the water will not escape the vesicle and will have the

same diffusivity as the vesicle or (ii) if the vesicles are permeable (i.e., unilamellar vesicles), the water molecules will escape after some time, within the experimental time.[30]

In the situation of fast exchange, if it is assumed that the monodisperse unilamellar vesicles which behave as hard spheres, an averaged self-diffusion coefficient of water, D_w, will be observed according to the two populations of water molecules, corresponding to inside and outside of the vesicles, with volume fractions P and $(1 - P)$, respectively.

$$D_w = PD_{ves} + (1 - P)AD_w^0 \qquad (5)$$

where D_{ves} and D_w^0 are the self-diffusion coefficients of entrapped and bulk water (i.e., the neat water self-diffusion coefficient), respectively. It is noteworthy that A is the excluded volume which in the case of hard spherical monodisperse vesicles is given by:

$$A = \left(1 + \frac{\phi_{ves}}{2}\right)^{-1} \qquad (6)$$

where ϕ_{ves} is the volume fraction of vesicles. For large vesicles (i.e., larger than the bilayer thickness), the fraction, P, corresponds to ϕ_{ves} and when the vesicles are so large that their diffusion can be neglected, we can obtain from the water reduced self-diffusion coefficient (D_w / D_w^0) the volume fraction of vesicles, ϕ_{ves}, according to[31]

$$\phi_{ves} = \frac{2\left(1 - \frac{D_w}{D_w^0}\right)}{2 + \frac{D_w}{D_w^0}} \qquad (7)$$

For large monodisperse single bilayer vesicles, the vesicle radius (R_{ves}) can be approximated from equation 8 as the surfactant length, l_s, is very small compared to R_{ves}.

$$R_{ves} = \frac{6\phi_{ves} l_s}{\phi_s} \qquad (8)$$

where ϕ_s is the surfactant volume fraction which can be related to the total surfactant molar concentration, C_T, by $\phi_s = N_A \times C_T \times v_s$, where N_A is the Avogadro number. It is noteworthy that l_s is defined as $l_s = v_s / a_s$, where v_s is the surfactant molecular volume and a_s is the area occupied by the

surfactant molecules at the interface (88 Å^2).[27] An estimation of the vesicle volume fraction and radius is given in Table 1. As depicted in Table 1, the averaged vesicle radius, R_{ves}, is around 106 ± 8 nm and it is close to the value obtained by SLS (R_g = 86 nm from Guinier analysis) and by DLS (R_h = 85.9 nm). This result support the formation of monodisperse unilamellar vesicles which behave as hard spheres.

Table 1. Estimated vesicle volume fraction, ϕ_{ves}, and vesicle radius, R_{ves}, obtained from the reduced water self-diffusion coefficients, D_w/D_w^0, as a function of **[DiC$_8$][Cl]** concentrations at 25 °C.

C_T (mM)	D_w/D_w^0 [a]	ϕ_{ves}	R_{ves} (nm)[b]
18	0.748	0.184	115
20	0.743	0.187	106
22	0.743	0.187	96

[a] The self-diffusion coefficient of neat water, D_w^0, is 2.30×10^{-9} m^2/s at 25 °C. [b] Calculated with a_s = 88 Å^2 and eqs. 7 and 8 (see earlier discussion).

Freeze-fracture transmission electron microscopy. In order to prove unambiguously the presence of vesicles in the 10-30 mM concentration range, freeze fracture-TEM imaging in this region have been performed. As depicted in Figure 7, freeze-fracture of **[DiC$_8$][Cl]** vesicles vary in appearance, depending on the fracture plane and on the structural heterogeneity of vesicles. Indeed, the vesicles may be convexly (Figures 7A and B), concavely (Figure 7D) or cross-fractured (Figure 7C). For instance, in Figure 7A, the external surface (ES) of a convexly fractured vesicle is seen. A similar vesicle in which the fracture has followed the external surface (ES) and then partially penetrated inside the bilayer of the vesicle is shown in Figure 7B leading to view innermost membrane (IS). Figure 7C illustrates examples in which the vesicles have been cross-fractured: the vesicle core (VC) appears relatively featureless. Despite these advantages, freeze-fracture technique has a serious drawback for estimating the vesicle size, the fracture plane passes through the sample but the vesicles are randomly positioned in the frozen section resulting in non mid plane fracture (see Figure 7). Consequently, the observed radius depends on the distance of the vesicle center from the plane of

the fracture, while the probability that a vesicle will be in the fracture plane depends on the vesicle radius. In any event, the vesicles look like spherical and the cross-fractured vesicles (where the plane of the fracture passes through the mid plane of vesicles) reveals a size compatible with the radii, R, determined from SLS, DLS, SANS and Self-diffusion NMR experiments (80 < R < 100 nm). It is noteworthy that additional micrographs are available in Supporting Information (Figures S1-S7).

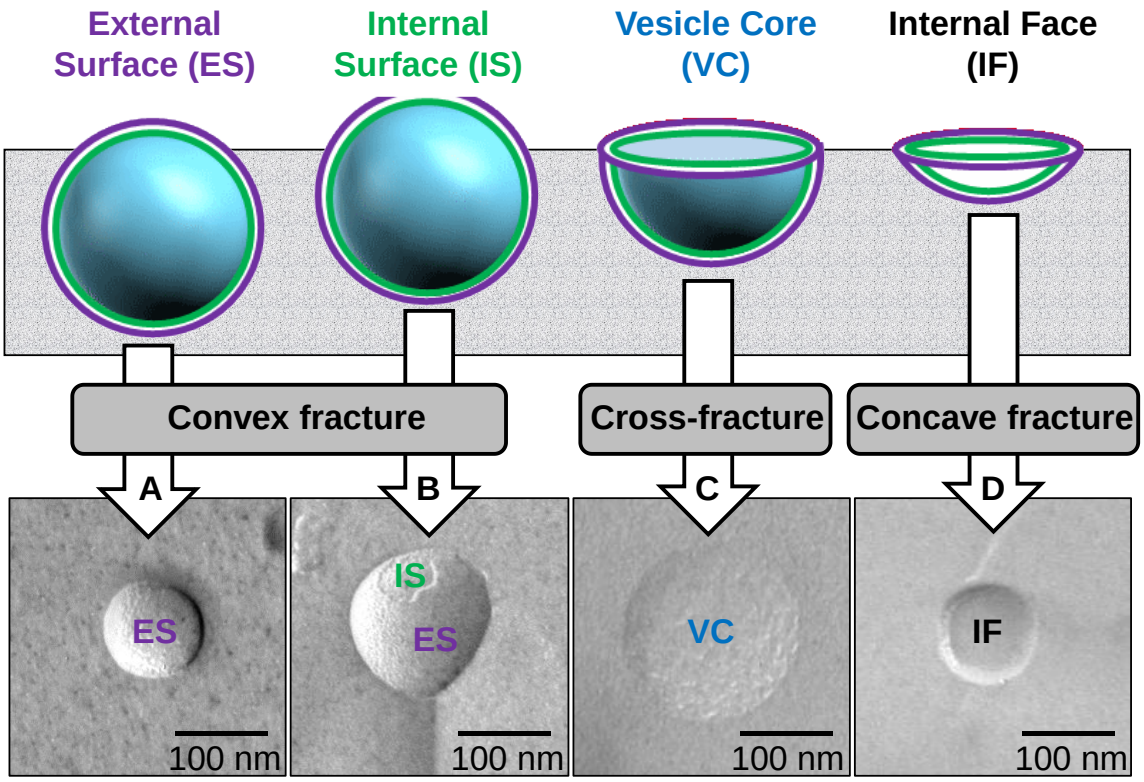

Figure 7. Freeze-fracture transmission electron micrographs of **[DiC$_8$][Cl]** aqueous solution (20 mM).

Supramolecular speciation from conductivity and SANS data treatment. In the following the amount of surfactant participating to the aggregates formed, dimer, vesicle and micelles will be estimated from the result obtained by the SANS spectra[28] and discussed together with the conductivity.

The conductivity curve was fitted by taking into account the following considerations and assumptions. The conductivity of **[DiC$_8$][Cl]** solutions can be expressed as the sum of contributions of dimers, micelles and vesicles as:

$$\kappa = [DiC_8][Cl]_{dim}\Lambda_{dim} + [DiC_8][Cl]_{ves}\Lambda_{ves} + [DiC_8][Cl]_{mic}\Lambda_{mic} \qquad (9)$$

where $\mathbf{[DiC_8][Cl]}_x$ and Λ_x are the surfactant concentration involved in the aggregate x and the specific conductivity of the aggregate x (with x = dimer, vesicle or micelle). Moreover, C_T = $\mathbf{[DiC_8][Cl]}_{dim}$ + $\mathbf{[DiC_8][Cl]}_{ves}$ + $\mathbf{[DiC_8][Cl]}_{mic}$. The contribution of the unimer to the conductivity is assumed to be negligible in the range of surfactant concentration used in the conductivity experiment. The critical dimer concentration (CDC) is indeed much lower than CAC_1 and CAC_2, CDC (0.1 mM) << CAC_1 < CAC_2, therefore for $\mathbf{[DiC_8][Cl]}$ > CDC then $\mathbf{[DiC_8][Cl]}_{unimer}$ << $\mathbf{[DiC_8][Cl]}$. The specific conductivity of the aggregates is related to their charge and size. As the vesicles are much larger than the dimers and vesicles, it can be assumed that $\Lambda_{ves} << \Lambda_{mic} < \Lambda_{dim}$.

For C_T < CAC_1, only dimers contribute to the conductivity, and Λ_{dim} can therefore be obtained from the conductivity curve (Λ_{dim} = 0.095 $mS.cm^{-1}.mM^{-1}$). For CAC_1 < C_T < CAC_2, we have C_T = $\mathbf{[DiC_8][Cl]}_{dim}$ + $\mathbf{[DiC_8][Cl]}_{ves}$. It can be observed that the slope in the conductivity curve (Figure 2b) does not change in the regions C_T < CAC_1 and CAC_1 < C_T < CAC_2. This may indicate that (i) the vesicles concentration is low compared to the dimer concentration because the vesicles do not contribute to the conductivity due to their large size, and (ii) the dimer concentration continuously increases in the regions C_T < CAC_1 and CAC_1 < C_T < CAC_2.

In order to check these hypothesis, information on the concentrations of dimers and vesicles can be obtained from the fit results of the SANS spectra at C_T = 10 and 20 mM.[28] It was shown that the two SANS spectra at 10 and 20 mM, obtained from plotting the absolute scattered intensity normalized by the surfactant concentration versus q, completely overlap over the whole q-range. This indicates that in the concentration range CAC_1 < C_T < CAC_2, $\mathbf{[DiC_8][Cl]}_{dim}$ and $\mathbf{[DiC_8][Cl]}_{ves}$ both increase in the same way, i.e., by keeping the $\mathbf{[DiC_8][Cl]}_{dim}$/$\mathbf{[DiC_8][Cl]}_{ves}$ ratio constant. The molar fraction of surfactant involved in the formation of vesicles can be defined as:

$$\alpha = \frac{[DiC_8][Cl]_{ves}}{[DiC_8][Cl]_{ves} + [DiC_8][Cl]_{dim}} \qquad (10)$$

where C_T = $\mathbf{[DiC_8][Cl]}_{dim}$ + $\mathbf{[DiC_8][Cl]}_{ves}$ in the range CAC_1 < C_T < CAC_2. The dimer concentrations for 10 and 20 mM surfactant solutions were previously determined: 2.35×10^{-3} and 4.7×10^{-3}

dimer/nm^3 which corresponds to **[DiC$_8$][Cl]**$_{dim}$ = 7.8 and 15.61 mM.[28] The molar fraction, α, can therefore be calculated α = 0.22 (7.8/10 and 15.61/20).

By taking all these considerations into account, a model for fitting the conductivity curve can be expressed by the following set of equations:

$$\kappa = \begin{cases} \Lambda_{dim} C_T \\ \Lambda_{dim} CAC_1 + (C_T - CAC_1)[\Lambda_{ves}\alpha + \Lambda_{dim}(1-\alpha)] \\ \Lambda_{di} CAC_1 + (CAC_2 - CAC_1)[\Lambda_{ves}\alpha + \Lambda_{dim}(1-\alpha)] + (C_T - CAC_2)\Lambda_{mic} \end{cases}$$

$$\text{for} \begin{cases} CDC << C_T < CAC_1 \\ CAC_1 < C_T < CAC_2 \\ C_T > CAC_2 \end{cases} \qquad (11)$$

where C_T is the surfactant concentration and *dim*, *mic* and *ves* stand for dimer, micelle and vesicle. In equation 11, the fitting procedure of the experimental data only considers then one fitting parameter, Λ_{mic}, as the other parameters could be determined separately. The conductivity curve can be well fitted by using this model (see Figure 8). Therefore the conductivity and SANS measurement are in good agreement confirming that only a small fraction of the surfactant participate in the formation of the vesicles, i.e., 22% of the surfactant in the range $CAC_1 < C_T < CAC_2$. Consequently, the other fraction of surfactant participates in the formation of dimers observed in the vesicle core (see above).

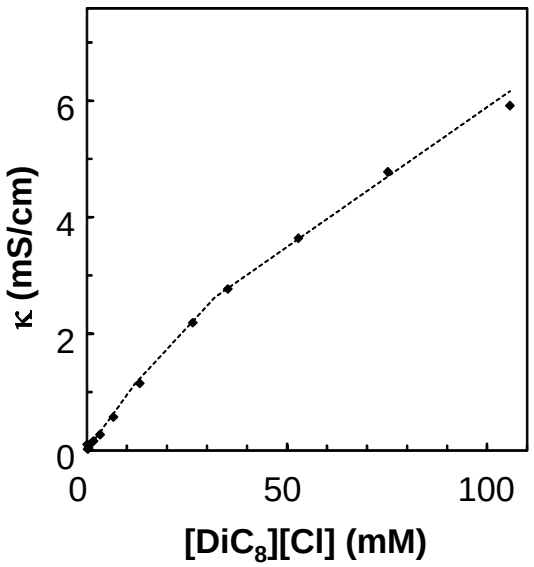

Figure 8. Experimental (◆) and calculated (dashed line) specific conductivity, κ, as a function of total **[DiC$_8$][Cl]** concentration, C_T, at 25.0 °C (see eq. 11 for more details).

Proposed mechanism. As previously mentioned, transitions from vesicles to micelles by increasing concentration are usually observed for surfactant mixtures systems (see above). Moreover, simple considerations using the packing parameter concept enables to predict such a phase transition by changing parameters such as pH, salt concentrations, etc. For water/pure surfactant binary mixtures vesicle-to-micelle transition has never been reported. In the last years a family of non-classical amphiphilic boron-based macro-anions (~1 nm in size), the metallacarboranes (MCs), has attracted much attention.[32-35] These anions, although lacking the classical hydrophilic-hydrophobic sequence of surfactants, have shown surfactant behaviors: micelle/vesicle formation,[32] lyotropic lamellar phase formation,[33] foaming,[34] surface activity.[35] It was shown that cobalt bis(diarbollide), the archetype molecule of MCs, presents a vesicle-to-micelle transition in binary mixtures with water by increasing concentration.[32] A mechanism based on Coulombic explosion was proposed recently to explain this counterintuitive transition.[33,34] For the present surfactant system, a similar mechanism can be proposed to explain the origin of the vesicles to micelles transition. Indeed vesicles are also formed here at lower concentrations than micelles, indicating that vesicles are of lower free energy than micelles. Therefore the spontaneous packing parameter of **[DiC$_8$][Cl]** is around one and leads to the formation of vesicles. The increase in the vesicle concentration, observed by SANS and confirmed by conductivity for $CAC_1 < C_T < CAC_2$, leads then to electrostatic repulsions between the vesicles because of their charge. Increase in the vesicle-vesicle repulsions, i.e., when Debye length starts to overlap, i.e., when C ~ CAC2, leads to increase tremendously the energy of the system which is then released by formation of (small) micelles. In order to check this hypothesis, the CAC_1/CAC_2 was determined (Figure 2d) in the presence of background salt ([NaCl] = 0.1 M) which aims at screening the vesicle-vesicle electrostatic repulsions. It was found that the addition of salt leads to increase the domain of existence of vesicles, as a consequence of a screening effect, which is in agreement with the proposed mechanism.

Another surprising behavior is the formation of dimers at low concentrations. The low dimer concentration indicates that monomers tend to decrease their free energy by forming dimers. This

may be a way for the surfactants to decrease the hydrophobic/water contact between the two bulky alkyl chains in water. Therefore, dimers, formed by a tail-tail self-assembly process, can be seen as the building block of the more complex aggregates: unimers → dimers → vesicles.

Conclusion.

We reported here convergent evidences for the abrupt unprompted edification of **[DiC$_8$][Cl]** vesicles at low concentrations after the surface saturation (CAC_1 = 10 mM), followed by an unexpected transition into micelles (CAC_2 = 30 mM). These vesicles were fully characterized by dynamic and static light scattering, self-diffusion NMR and freeze-fracture transmission electron microscopy whereas the micelles have been previously described from small-angle neutron scattering.[28] As **[DiC$_8$][Cl]** is known to form spontaneously dimers at very low concentrations (1-10 mM) in order to minimize the area of contact between the water molecules and the nonpolar alkyl tails of the surfactant (i.e., under the well-known hydrophobic effect), we can reasonably supposed that dimers represent ideal building blocks for the spontaneous formation of vesicles at CAC_1.[27] However, electrostatic repulsions between vesicles increase with concentration resulting in a mechanism close to Coulombic explosion into micelles at CAC_2. This unusual behavior is totally ascribed to the hydrophilic-hydrophobic balance of **[DiC$_8$]** cation which constitutes a borderline case between hydrotropes, ≤ **[DiC$_6$]**, and surfactants, ≥ **[DiC$_{10}$]**. This particular character leads to a contradiction between two features (i) the double chain structure tending to form planar aggregates with low water solubility, and (ii) the relatively short chains giving high hydrophilicity. Due to the current interest in the development of switchable drug delivery systems, fruitful developments are expected for pharmaceutical formulations with unusual supramolecular sequences.

Experimental section.

Materials. All the reagents were purchased from Sigma-Aldrich chemicals and used without further purification. All products were dried in a Freeze Dryer (Alpha 1-2 LD plus). In all experiments, the water used was Millipore (18.2 MΩ/cm; Simplicity 185).

Synthesis. The synthesis of dimethyl-di-*n*-octylammonium chloride, **[DiC$_8$][Cl]**, was prepared as previously described.[27] The purity of **[DiC$_8$][Cl]** obtained by this method was ≥ 99.9% only moisture trapped in the sample are observed due to hygroscopic nature of this salts (^{1}H NMR and elemental analysis).[27] ^{1}H NMR (300 MHz, $CDCl_3$, 20 °C, TMS): δ (ppm) = 0.86-0.90 (m, 6H; CH_3), 1.27-1.36 (m, 20H; CH_2), 1.69 (m, 4H; N-CH_2-CH_2), 3.43 (s, 6H; NCH_3), 3.50 (m, 4H; NCH_2). ^{13}C NMR (75 MHz, $CDCl_3$, 20 °C): δ (ppm) = 14.0, 22.5, 22.7, 26.2, 29.0, 29.1, 31.6, 51.3, 63.6. Anal. Calc. for ($C_{18}H_{40}NCl$); 1/3H_2O: C, 69.30%; H, 13.14%; N, 4.49%; O, 1.71%; Cl, 11.36%. Found: C, 68.96%; H, 13.57%; N, 4.46%; O, 1.79%; Cl, 11.18%. mp 75 °C. (Yield 96%). It is noteworthy that **[DiC$_8$][Cl]** was dried and store under dry nitrogen.^{1}H

Surface tension measurements. The tensiometer K100MK2 (Krüss) and the Wilhelmy plate method have been used for the surface tension measurements. A concentrated solution was prepared and the addition of small volumes to ultrapure water (σ = 72.0 mN.m^{-1} at 25 °C) was used to increase the solution concentration. After each addition, the solution was gently stirred for 30s. Equilibrium surface tension was measured for each concentration. All surface tension values were mean quantities of at least three measurements. The standard deviation of the mean never deviated ±1.5 % of the mean. The precision of the force transducer of the surface tension apparatus was 0.1 mN.m^{-1} and before each experiment, the platinum plate was cleaned in red/orange color flame. The temperature stabilization was estimated as better than ±0.05 °C with a thermoregulated bath.

Conductivity measurements. Conductance measurements were taken with a CDM210 conductivity meter (Radiometer). All measurements were taken in a thermostated water bath. The temperature stabilization was estimated as better than ±0.05 °C with a thermoregulated bath. The conductance was measured for each surfactant concentration after a sufficient time to reach a constant value. The maximum error limit of conductance measurements was ± 0.5%.

Solubility of hydrophobic dye. Solubility measurements were performed at 25.0 or 45.0 °C. For all **[DiC$_8$][Cl]** solutions (with or without NaCl, 0.1 M), Sudan II was added in excess. These solutions were mixed in a temperature-controlled water batch. After equilibration (72 h), these

solutions were filtered and the Sudan II solubility was determined by measuring the absorbance of diluted solutions at 543 nm with Cary 50 UV–visible spectrophotometer (Varian). Solubility (in arbitrary units, a.u.) was obtained by multiplying the absorbance of diluted solutions by the dilution factor.

Isothermal titration calorimetry. ITC experiments were performed using a nano-ITC titration calorimeter from TA Instruments at 25 °C. A 250 μL injection syringe was used with stirring at 400 rpm. **[DiC$_8$][Cl]** was dissolved in deionized water and the solutions were degassed gently under vacuum before use. Each titration comprised 25 × 10 μL injections of **[DiC$_8$][Cl]** (265 mM) into deionized water (950 μL). Control experiment with deionized water into deionized water was used to correct titration data.

Dynamic and static light scattering. The measurements used a 3D spectrometer (LS Instruments, Fribourg, Switzerland) equipped with a 25 mW HeNe laser (JDS uniphase) operating at 632.8 nm, a two channel multiple tau correlator, a variable-angle detection system, and a temperature-controlled index matching vat. The scattering spectrum was measured using two single mode fiber detections and two high sensitivity APD detectors (SPCM-AQR-13-FC, Perkin Elmer). The sample were filtered through 0.2 μm filter before its transfer into a cylindrical scattering cell. Each experiment was performed in triplicate to ensure reproducibility.

DOSY measurements. The self-diffusion coefficient of the nonionic surfactants were determined by the pulsed-field gradient NMR (PGSE-NMR) technique, by monitoring the ^{1}H signal on a Bruker Avance 500 spectrometer equipped with a field gradient probe unit. This method was first introduced by Stejskal and Tanner,[36] and in our experiments the BPP-STE-LED sequence,[37] combining constant time, bipolar pulse, stimulated echo, and the longitudinal eddy current delay method, was used.

Freeze-fracture transmission electron microscopy. Freeze-fracture samples were prepared by first depositing the sample (aqueous solution of **[DiC$_8$][Cl]** = 20 mM) on a gold tablet containing a

small well. The samples were frozen by plunging the sample into a liquid propane (-200 °C). The frozen sample was transferred to the sample block of a freeze-fracture device (Leica BAF 060). After temperature and pressure equilibration, the sample was fractured with knife and the resulting surfaces were replicated with platinum and carbon (≈ 30 nm). The replicas were washed in water and ethanol mixture in order to dissolve any remaining surfactant. The replicas were collected on copper TEM grids and observed using a Hitachi H600 transmission electron microscope at 75 KeV. The experiment was performed twice to ensure reproducibility.

Associated content.

Supporting Information

Copies of ^{1}H and ^{13}C NMR spectra. Seven additional freeze-fracture transmission electron micrographs. This material is available free of charge via the Internet at http://pubs.acs.org.

Author information.

Corresponding authors

*E-mail: loic.leclercq@univ-lille1.fr (L.L.)

*E-mail: veronique.rataj@univ-lille1.fr (V.N.-R.)

Author Contributions

All authors contributed equally to this work and approved the final version of the manuscript.

Notes

The authors declare no competing financial interest.

Acknowledgements.

Chevreul Institute (FR 2638), Ministère de l'Enseignement Supérieur et de la Recherche, Région Hauts-de-France and Fonds Européen de Développement Régional (FEDER) are acknowledged for supporting and funding partially this work.

References.

(1) Schneider, H. J.; Yatsimirsky, A. *Principles and Methods in Supramolecular Chemistry*, Wiley-VCH: Weinheim, **2000**.

(2) Steed, J. W.; Atwood, J. L. *Supramolecular Chemistry*, Wiley: Chichester, **2000**.

(3) Lehn, J.-M. *Supramolecular Chemistry. Concepts and Perspectives,* VCH: Weinheim, **1995**.

(4) Borovkov, V. V.; Hembury, G. A.; Inoue, Y. The origin of solvent-controlled supramolecular chirality switching in a bis(zinc porphyrin) system. *Angew. Chem., Int. Ed. Engl.* **2003**, *42*, 5310-5314.

(5) Xu, H.; Stampp S. P.; Rudkevich, D. M. A pH switch in supramolecular polymeric capsules. *Org. Lett.* **2003**, *5*, 4583-4586.

(6) Israelachvili, J.; Mitchell, D.; Ninham, B. Theory of self-assembly of hydrocarbon amphiphiles into micelles and bilayers. *J. Chem. Faraday Trans.* **1976**, *2*, 1525-1568.

(7) Nagarajan, R. Molecular Packing Parameter and Surfactant Self-Assembly. The neglected role of the surfactant tail, *Langmuir*, **2002**, *18*, 31-38.

(8) Kaler, E. W.; Murthy, K. A.; Rodriguez, B. E.; Zasadzinski, J. A. N. Spontaneous vesicle formation in aqueous mixtures of single-tailed surfactants. *Science* **1989**, *245*, 1371-1374.

(9) Zemb, T.; Dubois, M.; Deme, B.; Gulik-Kryzwicki, T. Self-assembly of flat nanodiscs in salt-free catanionic surfactant solutions. *Science* **1999**, *283*, 816-819.

(10) Khan, A.; Marques, E. F. Synergism and polymorphism in mixed surfactant systems. *Curr. Opin. Colloid Interface Sci.* **2000**, *4*, 402-410.

(11) Malmsten, M. *Surfactants and polymers in drug delivery*. Marcel Dekker, Inc: New York, **2002**.

(12) Renoncourt, A.; Bauduin, P.; Nicholl, E.; Touraud, D.; Verbavatz, J.-M.; Dubois, M.; Drechsler, M.; Kunz, W. Spontaneous vesicle formation of an industrial single-chain surfactant at acidic pH and at room-temperature *ChemPhysChem* **2006**, *7*, 1892-1896.

(13) Stuart, M. C. A.; Boekema, E. J. Two distinct mechanisms of vesicle-to-micelle and micelle-to-vesicle transition are mediated by the packing parameter of phospholipid-detergent systems. *Biochim. Biophys. Acta* **2007**, *1768*, 2681-2689.

(14) Yin, H.; Zhou, Z.; Huang, J.; Zheng, R.; Zhang, Y. Temperature-induced micelle to vesicle transition in the sodium dodecylsulfate/dodecyltriethylammonium bromide system. *Angew. Chem., Int. Ed.* **2003**, *42*, 2188-2191.

(15) Oberdisse, J.; Regev, O.; Porte, G. Experimental study of the micelle-to-vesicle transition. *J. Phys. Chem. B* **1998**, *102*, 1102-1108.

(16) Viseu, M. I.; Edwards, K.; Campos, C. S.; Costa, S. M. B. spontaneous vesicles formed in aqueous mixtures of two cationic amphiphiles. *Langmuir*, **2000**, *16*, 2105-2114.

(17) Jiang, L.; Wang, K.; Deng, M.; Wang, Y.; Huang, J. Bile salt-induced vesicle-to-micelle transition in catanionic surfactant systems. Steric and electrostatic interactions. *Langmuir* **2008**, *24*, 4600-4606.

(18) Philp, D.; Stoddart, J. F. Self-assembly in natural and unnatural systems. *Angew. Chem., Int. Ed.* **1996**, *35*, 1154-1196.

(19) Tian, M.; Fan, Y.; Ji, G.; Wang, Y. Spontaneous aggregate transition in mixtures of a cationic gemini surfactant with a double-chain cationic surfactant. *Langmuir* **2012**, *28*, 12005-12014.

(20) Leclercq, L.; Dewilde, A.; Aubry, J.-M.; Nardello-Rataj, V. Supramolecular assistance between cyclodextrins and didecyldimethylammonium chloride against enveloped viruses. Toward eco-biocidal formulations. *Int. J. Pharm.* **2016**, *512*, 273-281.

(21) Kuniega, H.; Shinoda, K. Solution behavior of dialkyldimethylammonium chloride in water. Basic properties of antistatic fabric softeners. *J. Phys. Chem.* **1978**, *82*, 1710-1714.

(22) Warr, G. G.; Sen, R.; Evans, D. F.; Trend, J. E. Microemulsion formation and phase behavior of dialkyidimethylammonium bromide surfactants. *J. Phys. Chem.* **1988**, *92*, 774-783.

(23) Kunitake, T.; Okahata, Y. A totally synthetic bilayer membrane. *J. Am. Chem. Soc.* **1977**, *99*, 3860-3861.

(24) Fontana, A.; De Maria, P.; Siania, G.; Robinson, B. H. Kinetics of breakdown of vesicles from didodecyldimethylammonium bromide induced by single chain surfactants and by osmotic stress in aqueous solution. *Colloid Surf. B* **2003**, *32*, 365-374.

(25) Soltero, J. F. A.; Bautista, F.; Pecina, E.; Puig, J. E.; Manero, O.; Proverbio, Z.; Schulz, P. C. Rheological behavior in the didodecyldimethylammonium bromide/water system. *Colloid Polym. Sci.* **2000**, *278*, 37-48.

(26) Hong, B.; Lai, J.; Leclercq, L.; Collinet-Fressancourt, M.; Aubry, J.-M.; Bauduin, P.; Nardello-Rataj, V. Binary and ternary phase behaviors of short double-chain quaternary ammonium amphiphiles. surface tension, polarized optical microscopy, and SAXS investigations. *J. Phys. Chem. B* **2013**, *117*, 14732-14742.

(27) Leclercq, L.; Nardello-Rataj, V.; Turmine, M.; Azaroual, N.; Aubry, J.-M. Stepwise aggregation of dimethyl-di-*n*-octylammonium chloride in aqueous solutions. From dimers to vesicles. *Langmuir* **2010**, *26*, 1716-1723.

(28) Collinet-Fressancourt, M.; Leclercq, L.; Bauduin, P.; Aubry, J.-M.; Nardello-Rataj, V. Counter anion effect on the self-aggregation of dimethyl-di-*n*-octylammonium cation. A dual behavior between hydrotropes and surfactants. *J. Phys. Chem. B* **2011**, *115*, 11619-11630.

(29) Burchard, W.; Richtering, W. Dynamic light scattering from polymer solutions. *Prog. Colloid Polym. Sci.* **1989**, *80*, 151-163.

(30) Silva, B. F. B.; Eduardo F. Marques, E. F.; Olsson, U. Unusual vesicle-micelle transitions in a salt-free catanionic surfactant. Temperature and concentration effects. *Langmuir* **2008**, *24*, 10746-10754.

(31) Olsson, U.; Nakamura, K.; Kunieda, H.; Strey, R. Normal and reverse vesicles with nonionic surfactant. Solvent diffusion and permeability. *Langmuir* **1996**, *12*, 3045-3054.

(32) Bauduin, P.; Prevost, S.; Farras, P.; Teixidor, F.; Diat, O.; Zemb, T. A Theta-shaped amphiphilic cobaltabisdicarbollide anion. Transition from monolayer vesicles to micelles. *Angew. Chem. Int. Ed.* **2011,** *50*, 5298-5300.

(33) Brusselle, D.; Bauduin, P.; Girard, L.; Zaulet, A.; Vinas, C.; Teixidor, F.; Ly, I.; Diat, O. lyotropic lamellar phase formed from monolayered theta-shaped carborane-cage amphiphiles. *Angew. Chem. Int. Ed.* **2013** *52*, 12114-12118.

(34) Vinas, C.; Tarres, M.; Gonzalez-Cardoso, P.; Farras, P.; Bauduin, P.; Teixidor, F. Surfactant behavior of metallacarboranes. A study based on the electrolysis of water. *Dalton Trans.* **2014**, *43*, 5062-5068.

(35) Gassin, P.-M.; Girard, L.; Martin-Gassin, G.; Brusselle, D.; Jonchère, A.; Diat, O.; Viñas, C.; Teixidor, F.; Bauduin, P. Surface activity and molecular organization of metallacarboranes at the air-water interface revealed by nonlinear optics. *Langmuir* **2015**, *31* 2297-2303.

(36) Stejskal, O. E.; Tanner, J. E. Spin diffusion measurements. Spin echoes in the presence of a time-dependent field gradient. *J. Chem. Phys.* **1965**, *42*, 288-292.

(37) Wu, D.; Chen, A.; Johnson, C. S. An improved diffusion-ordered spectroscopy experiment incorporating bipolar-gradient pulses. *J. Magn. Reson. Ser. A* **1995**, *115*, 260-264.

Graphical Abstract